PHYSICAL REVIEW C VOLUME 8, NUMBER 2 AUGUST 1973

Coupled-Channel-Born-Approximation Analysis of "Allowed" and "Forbidden" $^{22}Ne(p,t)^{20}Ne$ Transitions*

David K. Olsen, Takeshi Udagawa, and Taro Tamura
Center for Nuclear Studies, University of Texas, Austin, Texas 78712
and
Ronald E. Brown
John H. Williams Laboratory of Nuclear Physics, University of Minnesota, Minneapolis, Minnesota 55455
(Received 29 January 1973)

The effects of inelastic excitations on the $^{22}Ne(p,t)^{20}Ne$ reaction are investigated. Differential cross sections at a proton energy of 39.8 MeV were measured for $^{22}Ne(p,t)^{20}Ne$ transitions to the 0^+, 2^+, and 4^+ members of the ground-state rotational band, to the 2^- and 3^- members of the excited $K^\pi = 2^-$ band; and to the 0^+ and 2^+ members of the first excited $K^\pi = 0^+$ band. The cross sections to members of the ground-state band are compared with distorted-wave Born-approximation (DWBA) and coupled-channel-Born-approximation (CCBA) calculations using both pure Nilsson and pairing-mixed Nilsson rotational wave functions. Only the CCBA calculation with pairing provides a reasonable description of the experimental data. The effects of multistep processes are found to be as large for neon as for rare-earth nuclei. The shape and relative strength of the measured cross section to the 2^- state, a transition which is forbidden by a direct single-step process, are reproduced well by the CCBA calculation, which allows the excitation of the 2^- state by inelastic processes in the entrance and exit channels.

I. INTRODUCTION

Recently it has been shown that multistep processes which arise from inelastic excitations make very significant contributions to (p, t) cross sections. The coupled-channel-Born-approximation (CCBA) theory for explicitly calculating such effects was first formulated by Penny and Satchler.[1] They extended the usual distorted-wave Born-approximation (DWBA) formalism to include contributions from indirect processes. The amplitudes for these indirect processes add to the direct single-step DWBA amplitude and therefore contribute coherently to the cross section. Using formulations equivalent to that of Penny and Satchler,[1] CCBA calculations for (p, t) reactions have been reported for both spherical[2] and deformed[3-5] nuclei.

Even-even nuclei in the rare-earth region have been of particular interest for the initial investigation of these effects.[3-5] The magnitudes of the indirect amplitudes depend both upon the parentage of the states of interest and the strengths of the inelastic excitations, and both of these factors are large for rare-earth ground-state rotational bands. In addition, the basic simplicity of the nuclear structure of these bands allows accurate wave functions to be calculated. In these studies, initial and final state rotational wave functions of the adiabatic form have been used with intrinsic wave functions constructed from the mixing of a large number of Nilsson orbits by a simple pairing force.[6] CCBA calculations using such wave functions have reproduced both the experimental shapes and relative transition strengths remarkably well for such transitions.[4] In contrast, DWBA predictions have been in gross disagreement with the measured cross sections.

Neon is in another region of strong permanent deformation giving rise to rotational bands. In fact, the quadrupole deformations of the ground-state bands of ^{20}Ne and ^{22}Ne are considerably larger than those of rare-earth nuclei. Figure 1 shows all the low-lying levels of ^{20}Ne grouped into five rotational bands.[7] The adiabatic approximation appears to be valid, at least for the low-spin members of rotational bands in ^{20}Ne and ^{22}Ne. The ratios of electromagnetic matrix elements for the low-spin members of both ground-state bands and for the $K^\pi = 2^-$, ^{20}Ne excited band have been shown to be consistent with these states being generated from rigid rotations.[8] In addition, shell-model wave functions for these states overlap well with the corresponding wave functions projected from a single intrinsic state.[9] Hence transitions to low-spin members of the ^{20}Ne rotational bands provide excellent examples with which to investigate the effects of multistep processes on (p, t) reactions.

In this publication we report the measurement of $^{22}Ne(p, t)^{20}Ne$ differential cross sections at 39.8 MeV. In particular, angular distributions of transitions to the following ^{20}Ne states were obtained: the 0^+, 2^+, and 4^+ members of the $K^\pi = 0^+$, ground-state band; the 2^- and 3^- members of the first excited $K^\pi = 2^-$ band; and the 0^+ and 2^+ members of

the first excited $K^\pi = 0^+$ band. The experimental cross sections to members of the ground-state rotational band are compared with DWBA and CCBA calculations. Rotational wave functions with both pure Nilsson and pairing-mixed Nilsson intrinsic states are considered. Although the agreement is not perfect, only the pairing-mixed Nilsson wave functions with a full CCBA calculation provide a reasonable description of the data. The effects of the multistep processes are found to be as large for neon as for rare-earth nuclei. The CCBA calculation increases the 2^+ strength relative to the 0^+ strength almost an order of magnitude over that predicted by the DWBA.

The experimentally observed transition to the 2^- state at 4.97 MeV of excitation is not allowed by the selection rules resulting from the usual DWBA treatment[10] of (p, t) reactions. Other transitions from 0^+ targets to unnatural parity states have been observed in this region in violation of the selection rules.[11] In a previous note[12] we reported a CCBA calculation of relative (p, t) cross sections for transitions to the 2^-, 3^-, and 4^- members of the $K^\pi = 2^-$ rotational band in ^{20}Ne. In particular both the shape of the 2^- angular distribution and its strength relative to the 3^- transition were reproduced well. In this publication we expand the description of this work. For example the transition strengths of members of the $K^\pi = 2^-$ band relative to the ground-state band are calculated by considering the former intrinsic state to be a two-quasiparticle excitation of the latter intrinsic state.

Section II of this publication describes the experimental apparatus, procedure, and results. Section III gives an outline of the formalism used to calculate the two-neutron spectroscopic amplitudes and gives a brief description of our particular calculations. Finally, in Sec. IV a comparison of these calculations with the experimental data is discussed.

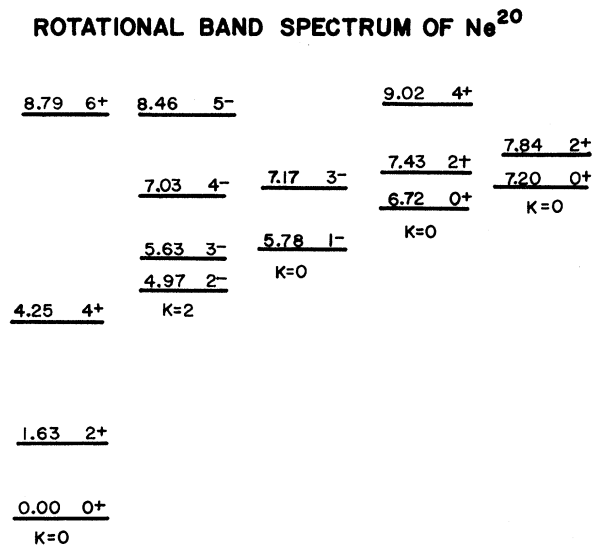

FIG. 1. All the low-lying energy levels of ^{20}Ne grouped into five rotational bands. Of particular interest here are the 0^+, 2^+, and 4^+ members of the $K^\pi = 0^+$, ground-state band; the 2^-, 3^-, and 4^- members of the excited, $K^\pi = 2^-$ band; and the 0^+ and 2^+ members of the first excited $K^\pi = 0^+$ band.

II. EXPERIMENTAL APPARATUS, PROCEDURE, AND RESULTS

A. Experimental Apparatus

The data were obtained by the bombardment of 99.4% isotopically pure ^{22}Ne gas with 39.8-MeV protons from the University of Minnesota proton linear accelerator. After passing through the target, the beam was collected in a small internal Faraday cup which was connected to a beam current integrating system and equipped with a small permanent magnet to reduce secondary electron scattering. Charged-particle reaction products were momentum analyzed by a vertical 100-cm radius, 180°, $n = \frac{1}{2}$, magnetic spectrometer, whose magnetic field was measured with a rotating-coil Gaussmeter. The 42-cm-diam scattering chamber was rigidly connected to the spectrometer and was attached to the input beam line by a vacuum sliding seal.

The momentum-analyzed reaction products were detected in an array of 32 surface-barrier detectors mounted in the focal plane of the magnetic spectrometer. These detectors were operated at an approximate depletion depth of 800 μm. Each detector had sensitive-area dimensions of 23 mm in the axial direction of the spectrometer and 5 mm in the radial direction. This gave an energy width along the focal plane of $0.0025E$ per detector, where E is the energy of the detected particle; therefore, the entire 32-detector array had an energy width of 8% of E. A 32-channel, pulse-height analysis was performed on the particle pulses from each detector. This was accomplished by biased amplification and discrimination in 32 parallel circuits and subsequent routing of the pulses into 32 subgroups of 32 channels each in a 1024-channel pulse-height analyzer.

The target gas was contained in a 5.1-cm-radius, 3.8-cm-high cylindrical gas cell which was equipped with a small extension out to a 7.6-cm radius to serve as a beam entrance port to allow data taking at small scattering angles. Havar foil of 2.5-μm thickness was used to cover the beam entrance port and exit window. These foils could hold a pressure of one atmosphere. The 1.0-cm-high exit cell windows allowed scattering angles

from −20 to +120° to be observed. The gas cell was supported within the scattering chamber and was connected to the outside by a hollow tube passing through the lid of the scattering chamber. This hollow tube allowed the cell to be filled or evacuated externally and the pressure to be measured by a simple Borden tube gage which was accurate to ±3 Torr. The gas-target geometry factor G[13] was defined both by an aperture 42.9-cm from the chamber center and by the walls of the magnetic spectrometer vacuum box. Normally, a 6.03-×0.95-cm aperture was used; however, a 3.81-×0.64-cm aperture was used for data taken at very forward angles.

B. Experimental Procedure

Particle types and energies of reaction products were determined by a knowledge of the magnetic field of the spectrometer and their energy loss in the focal-plane detectors. At the magnetic fields necessary to detect tritons, only tritons and deuterons were present in the focal-plane detector array, and both types of particles passed through the sensitive regions of the detectors. With both particle types passing, the pulse-height resolution then attainable made it impossible to separate tritons from an intense group of deuterons. Figure 2 shows the pulse-height distribution from a single array detector when only a weak triton group was present. In Fig. 2, 27-MeV tritons deposited about 11 MeV of energy in the detector, and the rise in the number of counts in the low channels was caused by neutron background.

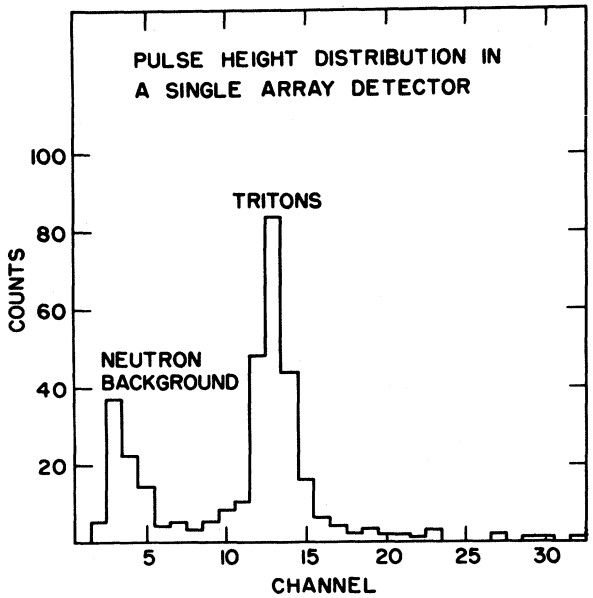

FIG. 2. Pulse-height distribution in a single focal-plane detector when only a weak triton group is incident upon it. The rise in the number of counts at small channels is background caused by neutrons.

Figure 3 shows ^{22}Ne$(p, t)^{20}$Ne survey spectra taken at 15 and 25°. With a ^{22}Ne gas-cell pressure of 508 Torr, an energy resolution (full width at half maximum) of 150 keV was obtained. The gaps in the spectra are due to intense deuteron groups which obscured the triton yield. All the levels below 7.84 MeV of excitation and the first $T = 1$ state at 10.27 MeV have been previously reported.

The errors shown for the differential cross sections in Figs. 4–10 are relative standard deviations. They include the statistical error from the number of counts, an estimate of the error due to background separation both in the pulse-height spectrum of a single detector and in summing the counts in a peak over a group of detectors, and, when necessary, an estimate of the error in separating the number of counts for two closely spaced peaks.

In addition to the relative error there is a standard deviation of ±5% in the absolute cross-section scale. This normalization error primarily is due to the uncertainty in the gas-target geometry factor G, whose numerical value was measured at several angles by the following three methods: (1) comparing H(p, p)H yields using pure hydrogen gas with the 40-MeV measurements of Johnston and Swenson[14]; (2) comparing ^{12}C$(p, ^3$He$)^{10}$B (g.s.) yields using gas (CH_4) and solid (CH_2) targets; (3) comparing ^{12}C$(p, t)^{10}$C (g.s.) yields, again using gas (CH_4) and solid (CH_2) targets. The walls of the spectrometer vacuum box proved to be completely adequate as a collimator to define a geometry suitable for gas targets. In addition, the inverse $\sin\theta$ dependence of the gas-target thickness was investigated by comparing yields from both solid and gas targets. Small corrections had to be made for deviations from this dependence at 10.0, 12.5, and 15.0°. Finally, the efficiency of the detector array as a function of detector number was investigated. At high magnetic fields a dropoff of efficiency at one end of the array was found to occur, and this region of the array was avoided during the measurement of angular distributions. More details of the experimental apparatus and procedures can be found elsewhere.[15]

C. Experimental Results

Figure 4 shows cross sections for the transitions to the 0^+, 2^+, and 4^+ members of the ground-state rotational band. Most of the data have rela-

tive errors of ±4%, which are roughly the size of the plotted points in the figure. It is interesting to note the relative transition intensities to members of this band; in particular, the 4^+ state is strongly excited. The 0^+, 2^+, and 4^+ transitions have intensities of 606, 68, and 45 μb/sr at the first maxima in their angular distributions which occur at 27, 35, and 30°, respectively.

Cross sections for the transitions to the 2^- and 3^- members at 4.97 and 5.63 MeV of excitation, respectively, of the first excited $K^\pi = 2^-$ band are shown in Fig. 5. As can be seen in the spectra of Fig. 3, the triton peak from the 3^- transition is not clearly resolved from that from the transition to the 1^- state at 5.80 MeV. However, the energy resolution available would have been sufficient to separate the two triton groups had the 1^- state been excited with any appreciable cross section. Because of the weakness of the 1^- transition, the triton peak in question reflects the transition strength to the 3^- state accurately enough for the analysis considered here. This is true at all angles for which data were obtained. It can also be seen in Fig. 3 that the "forbidden" transition to the 2^- state is roughly $\frac{1}{10}$ the strength of the "allowed" transition to the 3^- state and that the 2^- group is well isolated in the spectrum. There is no clear indication in Fig. 3 of a triton group to the 4^- member of this band at 7.03 MeV. In fact, the nearness of the triton group leading

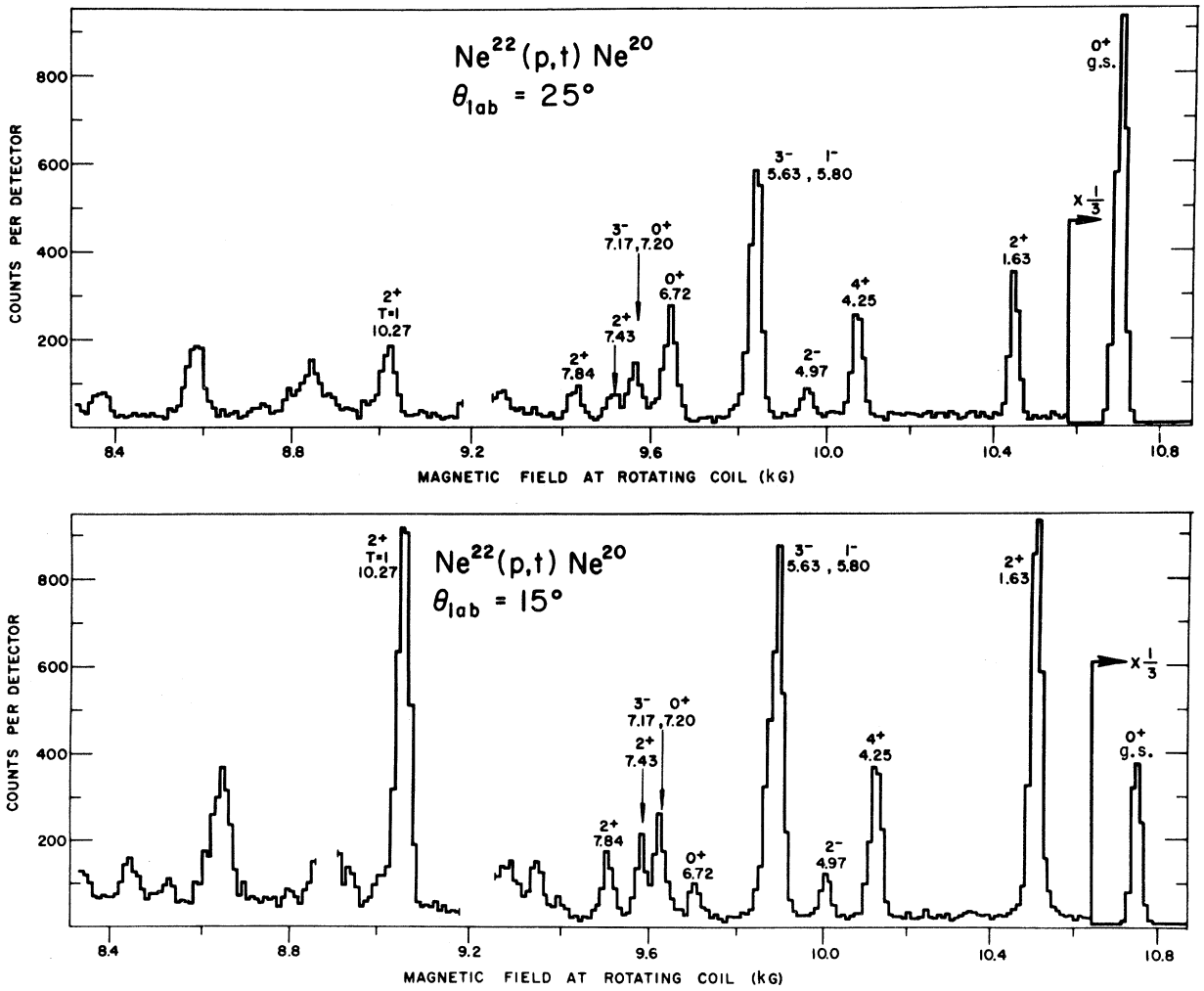

FIG. 3. ^{22}Ne$(p,t)^{20}$Ne survey triton spectra at 15 and 25°. The gaps in the spectra are due to intense deuteron groups which obscured the triton yield, and the smooth background is caused by neutrons. The states at 1.63 and 4.25 MeV are the 2^+ and 4^+ members of the ground-state rotational band. The 2^- and 3^- states at 4.97 and 5.63 MeV of excitation are rotational members of a well defined $K^\pi = 2^-$ band. The states at 6.72 and 7.43 MeV of excitation are the 0^+ and 2^+ members of the first excited $K^\pi = 0^+$ band.

to the 3^- state at 7.17 MeV prohibited us from making any cross section measurements to the 4^- state.

Figure 6 shows the measured cross sections for the transitions to the 0^+ and 2^+ members at 6.72 and 7.43 MeV, respectively, of the first excited $K^\pi = 0^+$ band in ^{20}Ne. These states are excited with roughly $\frac{1}{10}$ the strength of the corresponding states of the ground-state rotational band. The shape of the angular distribution to the excited 0^+ state is similar to the ground-state transition, whereas the shapes of the two 2^+ angular distributions deviate significantly from each other. This sharp difference in the shapes of the 2^+ transitions to the two different bands is attributed to the effects of inelastic excitations, and has recently been discussed by King *et al.*[5] The strong transition to the first $T=1$ state in ^{20}Ne has been studied in detail by Cerny, Pehl, and Garvey[16] and is not considered here.

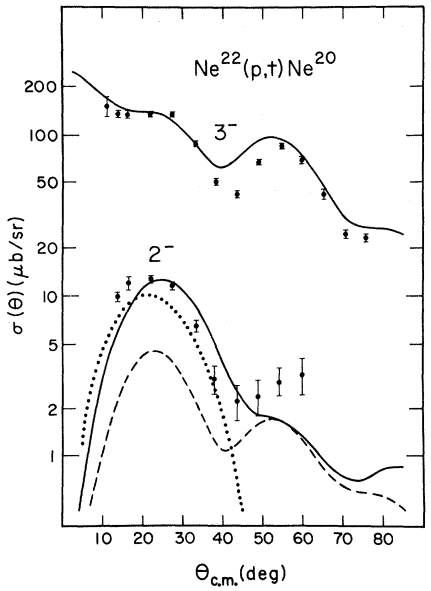

FIG. 5. Experimental differential cross sections for (p,t) transitions to the 2^- and 3^- members of the $K^\pi = 2^-$ band in ^{20}Ne. The solid curves are CCBA predictions for these transitions, and the dotted and dashed curves are separate contributions to the 2^- transition via the ^{22}Ne, 2^+ state and ^{20}Ne, 3^- state, respectively. The entire calculation was normalized to give the best visual fit to the 3^- cross section.

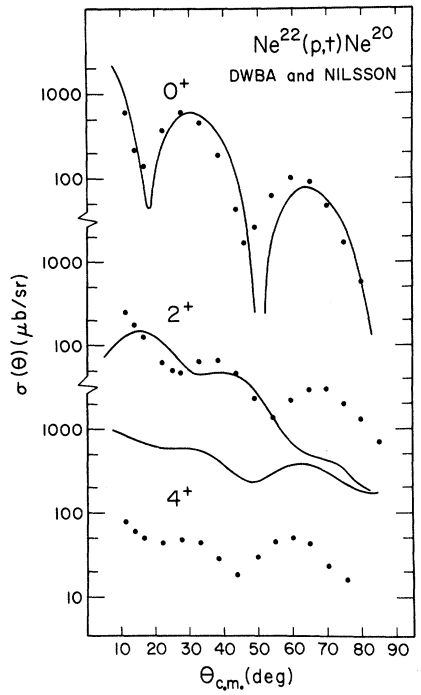

FIG. 4. Experimental differential cross sections for (p,t) transitions to the 0^+, 2^+, and 4^+ members of the ^{20}Ne ground-state band. At most angles the error bars are the size of the data points. The solid curves are DWBA predictions using pure Nilsson wave functions. The entire calculation was normalized to give the best visual fit to the 0^+ cross section. The calculated relative 4^+ strength is an order of magnitude larger than experimentally measured, and the fit to the 2^+ angular distribution is poor.

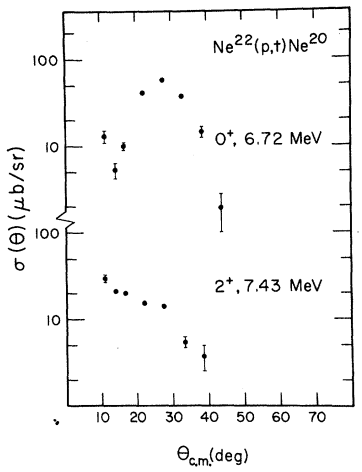

FIG. 6. Experimental differential cross sections at forward angles for (p,t) transitions to the 0^+ and 2^+ members of the first excited $K^\pi = 0^+$ band in ^{20}Ne. These states are excited with about $\frac{1}{10}$ the strength of the corresponding states in the ground-state band. The shape of the angular distribution of this 2^+ transition is considerably different from that to the ground-state band.

III. THEORY

A. Formalism for Two-Neutron Spectroscopic Amplitudes

The fundamental nuclear structure information involved in calculating (p, t) transition amplitudes are two-neutron spectroscopic amplitudes B. These amplitudes measure the overlap of the initial state of the target nucleus, $\Psi_{I_i}(A)$, with a state formed by coupling the residual nuclear state, $\Psi_{I_f}(A-2)$, to a spin-singlet two-neutron state of angular momentum J. If we define an operator $c^\dagger_{a_1}$ which creates a neutron in the spherical, single-particle state $a_1 \equiv (n_1 l_1 j_1)$, then B may be written[17]

$$B(I_i; a_1, a_2, J; I_f) = (-1)^{I_i + J - I_f} \left(\frac{2I_i+1}{2I_f+1}\right)^{1/2} \left\langle \Psi_{I_i}(A) \left| \left\{ \frac{[c^\dagger_{a_1} c^\dagger_{a_2}]^{\text{lab}}_J}{[1+\delta(a_1, a_2)]^{1/2}} \Psi_{I_f}(A-2) \right\}_{I_i} \right\rangle . \tag{1}$$

The general formalism for calculating these two-neutron spectroscopic amplitudes for (p, t) transitions between members of rotational bands has been discussed in detail in Ref. 6. We present only the basic assumptions and resulting equations of this formalism which are required for the specific (p, t) transitions considered here.

First, one assumes initial and final rotational nuclear wave functions of the adiabatic form,[18] that is

$$\Psi_{IKM} = \left(\frac{2I+1}{16\pi^2[1+\delta(K,0)]}\right)^{1/2} [D^I_{M,K}\chi_K + (-1)^{I+K} D^I_{M,-K}\chi_{\tilde{K}}], \tag{2}$$

where χ_K and $\chi_{\tilde{K}}$ are the intrinsic wave function and its time reversal, respectively. Using these wave functions and transforming the two-neutron wave function from the laboratory to the intrinsic coordinate

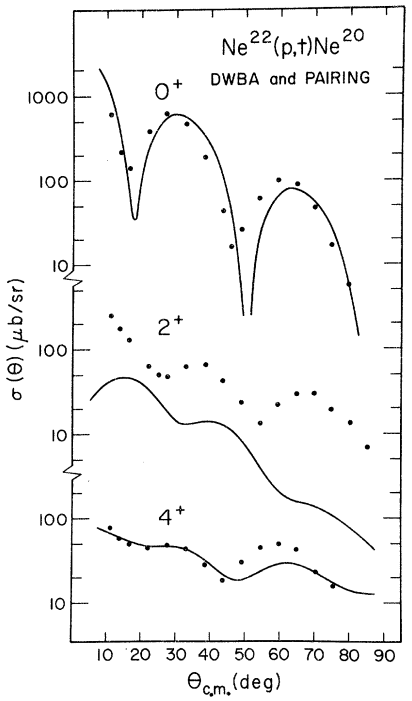

FIG. 7. Experimental differential cross sections for (p, t) transitions to the 0^+, 2^+, and 4^+ members of the ^{20}Ne ground-state band. The solid curves are DWBA predictions using pairing-mixed Nilsson wave functions. The entire calculation was normalized to give the best visual fit to the 0^+ cross section. The calculation does not predict correctly either the shape or relative strength of the 2^+ cross section.

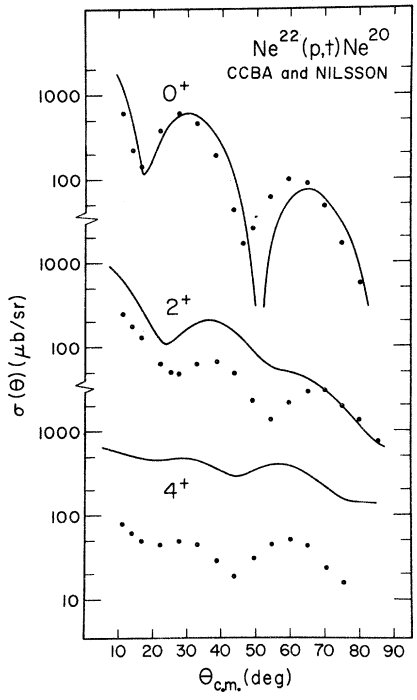

FIG. 8. Experimental differential cross sections for (p, t) transitions to the 0^+, 2^+, and 4^+ members of the ^{20}Ne ground-state band. The solid curves are CCBA predictions using pure Nilsson wave functions. The entire calculation was normalized to give the best visual fit to the 0^+ cross section. Both the relative 2^+ and 4^+ strengths are calculated to be considerably larger than experimentally measured.

system, one obtains

$$B(I_i, K_i=0; a_1, a_2, J; I_f, K_f)=\frac{2}{[1+\delta(K_f, 0)]^{1/2}}\left(\frac{2I_i+1}{2I_f+1}\right)^{1/2}\langle I_i 0 J K_f | I_f K_f\rangle B^{\text{intr}}(K_i=0; a_1, a_2, J; K_f). \quad (3)$$

We consider only transitions from a $K^\pi=0^+$ initial rotational band, and hence this formalism is only applicable to such cases. The $B^{\text{intr}}(0; a_1, a_2, J; K_f)$ are intrinsic two-neutron spectroscopic amplitudes and have the definition,

$$B^{\text{intr}}(0; a_1, a_2, J; K_f)=(-1)^{J+K_f}\left\langle \chi_{K_f}\left|\frac{[c_{a_1}^\dagger c_{a_2}^\dagger]^\dagger_{J,-K_f}}{[1+\delta(a_1, a_2)]^{1/2}}\right|\chi_0\right\rangle. \quad (4)$$

These amplitudes are evaluated from the intrinsic wave functions. They do not depend upon the specific angular momenta of the initial and final rotational states and hence only one set of such amplitudes need be evaluated for each J transfer allowed between the two bands.

The pairing-mixed Nilsson model is used to describe the intrinsic motion of the neutrons in the ground-state rotational wave functions. The pairing force is treated by the usual BCS method.[19] That is, the ground-state intrinsic wave functions are determined by using a pairing force of the form

$$Q=\frac{G}{4}\sum_{i>j} c_i^\dagger c_{\bar{i}}^\dagger c_j c_{\bar{j}} \quad (5)$$

to calculate occupation probabilities of neutron pairs in Nilsson, single-particle states. The operators $c_i^\dagger(c_i)$ create (annihilate) a neutron in the Nilsson orbit $i\equiv(N\omega r)$, where N is principle quantum number, ω is projection of the neutron angular momentum along intrinsic symmetry axis,

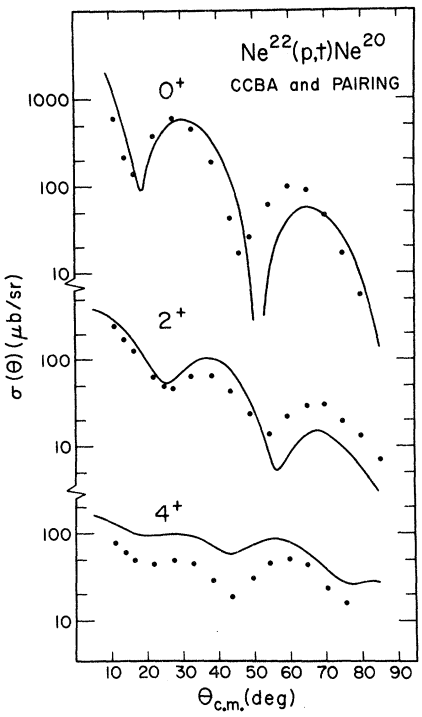

FIG. 9. Experimental differential cross sections for (p, t) transitions to the 0^+, 2^+, and 4^+ members of the ^{20}Ne ground-state band. The solid curves are CCBA predictions using pairing-mixed Nilsson wave functions. The entire calculation was normalized to give the best visual fit to the 0^+ cross section. The calculation fits all three angular distributions reasonably well.

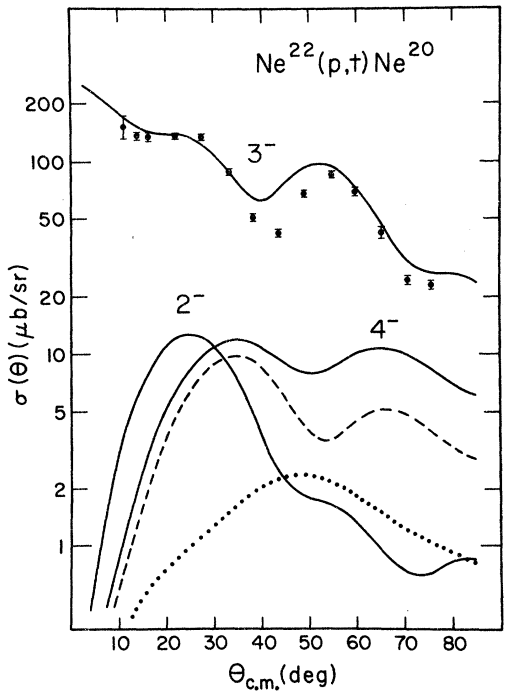

FIG. 10. Experimental differential cross sections for the (p, t) transition to the 3^- member of the $K^\pi=2^-$ band in ^{20}Ne. The solid curves are CCBA calculations for this transition and for the transitions to the 2^- and 4^- members of this band. The dotted and dashed curves are separate contributions to the 4^- transition via the ^{22}Ne, 2^+ state and the ^{20}Ne, 3^- state, respectively. The entire calculation was normalized to give the best visual fit to the 3^- cross section.

and r orders the single-particle states by energy ($\tilde{i}$ denotes the time reversal of state i).

Under the assumption that the initial and final intrinsic states have the same deformation, the intrinsic two-neutron spectroscopic amplitudes between the two ground-state bands are given by

$$B^{\mathrm{intr}}(0; a_1, a_2, J; 0) = \frac{1}{[1+\delta(a_1, a_2)]^{1/2}}[1+(-1)^{J+l_1+l_2}] \times \sum_{\omega_1>0}(-1)^{j_1+l_2+\omega_1} \times \langle j_1\omega_1 j_2 - \omega_1 | J0\rangle f^{\omega_1}_{a_1 a_2}, \quad (6)$$

where

$$f^{\omega_1}_{a_1 a_2} = \sum_i U_i(A-2)V_i(A)W^i_{a_1\omega_1}W^i_{a_2\omega_1}. \quad (7)$$

The quantities U_i and V_i are the pair probability amplitudes for the Nilsson state i to be empty or full, respectively. The amplitudes $W^i_{a\omega}$ are transformation coefficients between Nilsson and spherical single-particle states. That is,

$$c^\dagger_{a_1\omega_1} = \sum_i W^i_{a_1\omega_1}c^\dagger_i. \quad (8)$$

We also consider transitions to an excited rotational band. The intrinsic state of this excited band is constructed by a two-quasiparticle excitation of the BCS Nilsson ground-state vacuum. This is an intrinsic state of the form $d^\dagger_i d^\dagger_j|\tilde{0}\rangle$, where $|\tilde{0}\rangle$ is the BCS Nilsson vacuum and the operators $d^\dagger_i$ and $d^\dagger_j$ are Nilsson quasiparticle creation operators defined by

$$d^\dagger_i = U_i c^\dagger_i - V_i c_{\tilde{i}}, \quad (9)$$
$$d^\dagger_{\tilde{j}} = U_i c^\dagger_{\tilde{i}} + V_i c_i.$$

If the difference between initial and final correlated ground states is neglected, the intrinsic two-neutron spectroscopic amplitudes connecting the excited band to the ground-state band are given by

$$B^{\mathrm{intr}}(0; a_1, a_2, J; K_f) = \frac{1}{[1+\delta(a_1, a_2)]^{1/2}}\langle j_1\omega_1 j_2\omega_2 | JK_f\rangle \times \frac{1}{1+\delta(i,j)}(W^i_{a_1\omega_1}W^{\tilde{j}}_{a_2\omega_2} + W^i_{a_2\omega_2}W^{\tilde{j}}_{a_1\omega_1})V_iV_j, \quad (10)$$

where V_i and V_j are taken to be the average of those from ^{20}Ne and ^{22}Ne.

B. DWBA and CCBA Calculations

Both ^{20}Ne and ^{22}Ne have been extensively investigated and are known to be highly deformed. Quadrupole deformation parameters β_2 of 0.45 for both ground-state rotational bands are consistent with inelastic proton scattering data.[20] In addition, the ground-state band of ^{20}Ne is known to have a very large hexadecapole moment whereas ^{22}Ne does not.[20] In the construction of the BCS deformed intrinsic ground state all Nilsson single-particle neutron states arising from the $1s_{1/2}$, $1p_{1/2}$, $1p_{3/2}$, $1d_{5/2}$, $2s_{1/2}$, and $1d_{3/2}$ spherical states were considered. The Nilsson states were generated in a deformed oscillator potential well with a quadrupole deformation only and were expanded in spherical states from the same major harmonic-oscillator shell. The parameters of the Nilsson single-particle Hamiltonian[21] were: $\hbar\omega_0 = 41A^{1/3}$ MeV, $\kappa = 0.08$, $\mu = 0.00$, and $\delta = 0.43(\beta = 0.45)$. Such Nilsson states with band mixing describe well the properties of low-lying levels of odd-even nuclei in the neon region.[22]

The occupation probabilities for neutron pairs in the ten Nilsson orbits were calculated using a pairing force of strength $G = 28.0$ MeV. This strength gives an energy gap of about 2.0 MeV, which is equal to the odd-even neutron mass difference in this region. We consider a 0^+-2^+ coupling in the entrance channel. For transitions to the 0^+, 2^+, and 4^+ members of the ground-state band we allow a 0^+-2^+-4^+ coupling in the exit channel. Conservation of angular momentum then allows $J = 0$, 2, 4, and 6 for the (p, t) form factors connecting the initial and final states. Our basis states do not allow $J = 6$ transfers. Table I gives two-neutron spectroscopic amplitudes calculated from Eqs. (6) and (7) for the $J = 0$, 2, and 4

TABLE I. Pairing and Nilsson, intrinsic, two-neutron spectroscopic amplitudes B^{intr} of transferred angular momentum J to indicated ^{20}Ne rotational band.

J	n_1	l_1	$2j_1$	n_2	l_2	$2j_2$	$B^{\mathrm{intr}}_{\mathrm{pairing}}$	$B^{\mathrm{intr}}_{\mathrm{Nilsson}}$
				To $K^\pi = 0^+$ ground-state rotational band				
0	1	0	1	1	0	1	−0.0410	
	1	1	1	1	1	1	0.1664	
	1	1	3	1	1	3	0.1528	
	2	0	1	2	0	1	−0.2336	
	1	2	3	1	2	3	−0.3419	−0.0426
	1	2	5	1	2	5	−0.7731	−0.5425
2	1	1	1	1	1	3	−0.0584	
	1	1	3	1	1	3	0.0241	
	2	0	1	1	2	3	0.1574	
	2	0	1	1	2	5	−0.0004	
	1	2	3	1	2	3	0.1216	−0.0426
	1	2	3	1	2	5	−0.1776	−0.3116
	1	2	5	1	2	5	0.1515	0.1450
4	1	2	3	1	2	5	−0.2040	−0.1272
	1	2	5	1	2	5	0.3955	0.7534
				To $K^\pi = 2^-$ excited rotational band				
3	1	2	5	1	1	1	−0.4702	
	1	2	5	1	1	3	−0.0658	
	1	2	3	1	1	3	0.0408	

transitions between these ground-state intrinsic wave functions. Since it is not at all obvious that pairing is required for these light nuclei, we also consider pure Nilsson wave functions. In this case $G=0.00$, and the spectroscopic amplitudes arise from the transfer of two neutrons from Nilsson orbit No. 7 ($\omega=\frac{5}{2}$). These spectroscopic amplitudes are also given in Table I.

We also consider (p,t) transitions to the 2^-, 3^-, and 4^- members of the excited $K^\pi=2^-$ band and allow a 2^--3^--4^- coupling in the exit channel in addition to the 0^+-2^+ coupling in the entrance channel. Whereas conservation of angular momentum allows $J=1$, 3, and 5 form factors, our basis allows only $J=1$ and 3. The K selection rule forbids $J=1$ transfer, and hence we need calculate only one $J=3$ intrinsic form factor. This form factor is calculated by considering the 2^- intrinsic wave function to be a two-quasiparticle state. We assume that the state consists of Nilsson orbits No. 4 ($\omega=\frac{1}{2}$) and No. 7 ($\omega=\frac{3}{2}$), which yields the lowest-energy 2^- state in this model. Table I gives the spectroscopic amplitudes calculated from Eq. (10) for the $J=3$ transfer to this intrinsic state.

The two-neutron transfer form factors were calculated from the spectroscopic amplitudes using the computer code TWOPAR,[23] which uses a zero-range interaction between the incoming proton and dineutron center of mass. Whereas the deformed Nilsson states were based upon a spherical oscillator representation, the spherical single-particle bound-state wave functions of the transferred neutrons were generated in a Woods-Saxon potential well with a radius of $1.25(21)^{1/3}$ fm. The well had a diffuseness of 0.65 fm and a spin-orbit coupling of 30 times the Thomas term. The depth of this well was adjusted for each single-particle state to give a binding energy equal to one half the two-neutron separation energy from the ground state for the ground-state band and from the 3^- state for the excited band. These form factors were then used as input into the CCBA computer program MARS.[24]

Optical-model and deformation parameters used to generate the distorted waves are summarized in Table II. The optical-model parameters for the proton channel are those of Watson, Singh, and Segel.[25] These contain explicit energy and isospin terms for the potential depths and radii and give reasonable fits to 10- to 50-MeV elastic scattering data in the $1p$ shell. The proton parameters of Table II are quite similar to those obtained from an analysis[20] of cross-section and polarization data of 24.5-MeV protons on ^{22}Ne. The triton parameters are similar to those reported by Becchetti and Greenlees,[26] which were also determined by fitting a large sample of elastic scattering data. Similarly, the quadrupole and hexadecapole deformation parameters were taken from published experimental work,[20] with the exception of the quadrupole deformation of the excited ^{20}Ne band. This β_2 was taken to be about 20% larger than that of the ^{20}Ne ground-state rotational band. In the next section we compare these calculations with the experimental data.

IV. CALCULATED RESULTS AND DISCUSSION

A. $K^\pi=0^+$ Ground-State Rotational Band

Figures 4, 7, 8, and 9 show the various calculated cross sections for transitions to the 0^+, 2^+, and 4^+ members of the ground-state rotational band. The calculated curves are normalized to the experimental data to give the best visual fit to the 0^+ cross section, and the 2^+ and 4^+ cross sections are then given uniquely. Table III gives the experimental cross section and the absolute calculated cross sections of the ground-state angular distribution at the first maximum near 30° using a zero-range force constant D_0^2 equal to 26.2×10^4 MeV^2 fm^3. This force constant gives agreement between experiment and the CCBA with pairing calculation. Absolute normalization factors of similar magnitude have been reported by other workers for (p,t) transitions.[27]

Figure 4 shows the results of the DWBA calculation using the pure Nilsson model wave functions. The shapes of the 0^+ and 4^+ angular distributions are reproduced reasonably well by the calculation. However, the calculated strength of the 4^+ transition relative to that of the 0^+ transition is an order of magnitude larger than experimentally measured, and although the relative strength of the 2^+ transition is calculated correctly, the fit to the shape of this angular distribution is poor. In

TABLE II. Optical-model and deformation parameters.

Channel	r_R (fm)	a_R (fm)	V_R (MeV)	r_I (fm)	a_I (fm)	W_V (MeV)	W_D (MeV)	r_c (fm)	β_2	β_4
p	1.11	0.57	52.2	1.11	0.50	6.2	8.2	1.11	0.45	0.05
t	1.20	0.72	160.4	1.40	0.84	25.0	0.0	1.30	0.45 [a]	0.25

[a] $\beta_2=0.55$ was used for the excited $K^\pi=2^-$ band.

particular, at very forward angles the calculated cross section decreases, whereas the experimental cross section increases. In addition, the calculation fails to account for the second maximum at 65°.

Figure 7 shows the DWBA calculation using pairing-mixed Nilsson wave functions. As shown in Table III the pairing increases the 0^+ strength by a factor of 7.5. The relative 4^+ strength is now reproduced well whereas the 2^+ strength is predicted to be considerably smaller than that required by the data. In addition the shape of the 2^+ cross section is not significantly changed by the addition of the pairing and is still fitted poorly. The introduction of pairing into the DWBA calculation does not markedly improve the agreement with experiment.

The results of the CCBA calculations assuming pure Nilsson and pairing-mixed Nilsson wave functions are shown in Figs. 8 and 9, respectively. The addition of the multistep processes has little effect on the shapes of the 0^+ and 4^+ angular distributions and, as can be seen in Table III, does not significantly change the 0^+ absolute cross section. Although the CCBA using pure Nilsson model wave functions (Fig. 8) improves the fit to the shape of the 2^+ cross section, the calculation still fails to reproduce the second maximum. In addition these wave functions yield both 2^+ and 4^+ relative transitions strengths in strong disagreement with the experimental data.

On the other hand, the CCBA calculation with pairing-mixed Nilsson wave functions (Fig. 9) provides a reasonable description of the data. The shapes of all three angular distributions are reproduced, including the second maximum of the 2^+ cross section. Furthermore, this calculation reproduces the relative transition strengths better than do the other three calculations. The relative transition strength to the 2^+ state is given correctly, and the 4^+ relative strength is calculated to be twice as large as experimentally measured. It is interesting to note that the choice of model wave functions changes the shape of the 2^+ cross section with the CCBA but not with the DWBA. In addition, the pairing mixing provides a larger contribution from indirect processes.

TABLE III. Absolute differential cross sections for the $J=0$ ground-state angular distribution at the first maximum near 30° using a zero-range force constant $D_0^2 = 26.2 \times 10^4$ MeV^2 fm^3.

Experimentally measured	606 μb/sr
DWBA and Nilsson calculation	70 μb/sr
DWBA and pairing calculation	524 μb/sr
CCBA and Nilsson calculation	75 μb/sr
CCBA and pairing calculation	606 μb/sr

B. $K^\pi = 2^-$ First Excited Rotational Band

The calculated results for the 2^- and 3^- transitions are compared with the experimental cross sections in Fig. 5. The full curves are CCBA results for these transitions, whereas the dotted and dashed curves are the two most important individual components which contribute to the excitation of the 2^- state. These are the two-step paths via the ^{22}Ne, 2^+ state and ^{20}Ne, 3^- state, respectively. The selection rules do not allow the 2^- state to be excited directly from the ^{22}Ne ground state. The calculated curves are normalized to these data to give the best visual fit to the 3^- cross section. This required the 2^- and 3^- calculated cross sections to be multiplied by a factor of 1.12 relative to the ground-state transition. That is, the two-Nilsson quasiparticle model of the intrinsic $K^\pi = 2^-$ state accounts for 89% of the (p, t) strength to the 3^- state. The 3^- angular distribution is fitted well by the calculation, and the fit to the 2^- angular distribution is satisfactory. More important, as can be seen in Fig. 5, optical-model and deformation parameters consistent with elastic and inelastic scattering data reproduce well the ratio of the 2^- cross section to the 3^- cross section.

This ratio in our calculation is independent of the details of the initial and final intrinsic wave functions because the adiabatic approximation and our choice of basis states allow only one $J=3$ intrinsic form factor to connect rotational members of the initial and final bands. This ratio then does not depend on the absolute magnitude of this form factor since it contributes equally to all possible (p, t) paths connecting the two bands. Configuration mixing among the single-particle orbits allows only $(1d_{5/2}, 1p_{1/2})$, $(1d_{5/2}, 1p_{3/2})$, and $(1d_{3/2}, 1p_{3/2})$ orbital pairs in a $J=3$ form factor. All these orbital pairs have the same orbital angular momentum and radial nodes and hence give form factors of the same shape. Therefore, the relative intensities of the 2^-, 3^-, and 4^- transitions do not depend upon our particular calculation of the above three spectroscopic amplitudes. Only the (p, t) strength to the excited band relative to the ground-state band depends upon these numbers.

The amplitudes for the two main paths to the 2^- state of course contribute coherently. The path via the ^{22}Ne, 2^+ state contributes about two thirds of the 2^- strength and the path via the ^{20}Ne, 3^- state contributes the remaining third. In our calculation the ratio of the 2^- cross section to the

3^- cross section depends mostly on the quadrupole deformation parameters in the entrance and exit channels since these provide the paths by which the 2^- state is excited. We use a slightly larger β_2 for the excited band than the value for the ^{20}Ne ground-state band determined from inelastic scattering. There is no reason why the two rotational bands need be generated from the same intrinsic shape.

Our calculation of both the relative transition strength and angular-distribution shape of the 2^- state indicates that inelastic scattering is the main reaction mechanism by which this state is excited. The smooth curve in Fig. 10 shows our prediction of the cross section for the transition to the 4^- state of this band relative to the 3^- transition. The dotted and dashed curves are the individual components to this cross section from paths via the ^{22}Ne, 2^+ state and ^{20}Ne, 3^- state, respectively. The strength of the maximum of the 4^- cross section is roughly equal to that of the 2^- cross section, which is also shown in the figure. It would be of considerable interest for an experimental test to be made of this 4^- prediction. The angular distributions of both these "forbidden" transitions have shapes unlike those of any allowed transitions in this mass and energy region.

V. CONCLUSIONS

The CCBA calculation using the pairing-mixed Nilsson model wave functions in general successfully describe both the relative magnitudes and shapes of the "allowed" and "forbidden" ^{22}Ne(p, t)-^{20}Ne cross sections we have considered. The shapes of the 0^+, 2^+, 4^+, and 3^- "allowed" transitions are fitted reasonable well. The relative 2^+ transition strength is predicted correctly; however, the calculation gives twice the 4^+ strength that is required by the data. Perhaps this discrepancy is due to the lack of a hexadecapole term in the Nilsson single-particle Hamiltonian.[6] In addition the (p, t) relative strength to the excited $K^\pi = 2^-$ band has been given very well by assuming the intrinsic state to be a simple two-quasiparticle excitation of the pairing ground state. The CCBA with pairing has the largest effect on the shape and relative magnitude of the 2^+ transition. It is interesting to note that both the simplest calculation using the DWBA with pure Nilsson wave functions and the more sophisticated CCBA calculation with pairing predict the same relative 2^+ strength. However, only the latter calculation gives a reasonable fit to the shape of this angular distribution.

Perhaps the most interesting result obtained from this work is the CCBA calculation of cross sections to unnatural parity final states. The usual zero-range DWBA formalism[10] for (p, t) reactions does not allow the excitation of such states from 0^+ targets. In addition to conservation of angular momentum and parity, this selection rule results from the following three assumptions: (i) The reaction mechanism is that of a direct single-step process; (ii) the triton is described by a wave function in which the two neutrons have unit probability for having both zero total spin angular momentum and zero relative orbital angular momentum; (iii) the interaction between the proton and the picked-up neutrons depends only on the distance between the proton and the c.m. position of the two neutrons. Bayman and Feng[28] have performed a calculation in which assumptions (ii) and (iii) above were relaxed. They used a central interaction with both spin-independent and spin-dependent components. When they compare their calculation for the present 2^- transition with the data, they find the calculated cross section is several orders of magnitude too small, and does not reproduce the experimental shape as well as does the present calculation. The CCBA calculation, using realistic optical-model and deformation parameters, predicts well both the relative transition strength and shape of the experimental 2^- angular distribution. Much of this calculation is independent of the details of the intrinsic nuclear wave functions involved. We conclude that inelastic scattering is the main factor contributing to the excitation of this 2^- state. Many unnatural parity states in other energy and mass regions are probably also excited from 0^+ targets by the same process.

ACKNOWLEDGMENTS

The authors wish to thank Professor B. F. Bayman for making the computer code TWOPAR available to us and the entire technical staff of the John H. Williams Laboratory of Nuclear Physics for their help in the experimental aspects of this work. The assistance of D. Madland in the data taking is gratefully acknowledged.

---

*Work supported in part by the U. S. Atomic Energy Commission, contract Nos. AT-(11-1)-1265 and AT-(40-1)-2972.

[1]S. K. Penny and G. R. Satchler, Nucl. Phys. **53**, 145 (1963).

[2]N. K. Glendenning, in *Proceedings of the International Conference on Properties of Nuclear States*, edited by M. Harvey *et al.* (Les Presses de L'Universite de Montreal, Canada, 1969), p. 245; R. J. Ascuitto and N. K.

Glendenning, Phys. Rev. C **2,** 1260 (1970); T. Udagawa, T. Tamura, and I. Izumoto, Phys. Lett. **35B,** 129 (1971).

[3]T. Tamura, D. R. Bes, R. A. Broglia, and S. Landowne, Phys. Rev. Lett. **25,** 1507 (1970); Phys. Rev. Lett. **26,** 156(E) (1971); R. J. Ascuitto, N. K. Glendenning, and B. Sorensen, Phys. Lett. **34B,** 17 (1971).

[4]R. J. Ascuitto, N. K. Glendenning, and B. Sorensen, Nucl. Phys. **A183,** 60 (1972).

[5]C. H. King, R. J. Ascuitto, N. Stein, and B. Sorensen, Phys. Rev. Lett. **29,** 71 (1972).

[6]R. A. Broglia, C. Riedel, and T. Udagawa, Nucl. Phys. **A135,** 561 (1969).

[7]J. A. Kuehner and J. D. Pearson, Can. J. Phys. **42,** 477 (1964).

[8]O. Hausser, T. K. Alexander, A. B. McDonald, G. T. Ewan, and A. E. Litherland, Nucl. Phys. **A168,** 17 (1971); D. K. Olsen, W. R. Phillips, and A. R. Barnett, Phys. Lett. **39B,** 201 (1972).

[9]H. G. Benson and B. H. Flowers, Nucl. Phys. **A126,** 305 (1969); A. Arima, S. Cohen. R. D. Lawson, and M. H. MacFarlane, Nucl. Phys. **A108,** 94 (1968).

[10]N. K. Glendenning, Annu. Rev. Nucl. Sci. **13,** 191 (1963); B. Bayman, Argonne National Laboratory Report No. ANL-6848, 1964 (unpublished); N. K. Glendenning, Phys. Rev. **137,** B102 (1964); E. M. Henley and D. V. L. Yu, Phys. Rev. **133,** B1445 (1964); C. L. Lin and S. Yoshida, Prog. Theor. Phys. **32,** 885 (1965).

[11]J. R. Shepard, J. J. Kraushaar, and H. W. Baer, Phys. Rev. C **5,** 1288 (1972); the (p,t) excitation of the ^{20}Ne, 2^- state has also been reported by the Manitoba group: W. R. Falk, P. Kulisic, and A. McDonald, Nucl. Phys. **A167,** 157 (1971).

[12]D. K. Olsen, T. Udagawa, T. Tamura, and R. E. Brown, Phys. Rev. Lett. **29,** 1178 (1972). Equation (1) of this reference contains a typographical error. The spin factor of Eq. (1) should be $[(2I_i + 1)/(2I_f + 1)]^{1/2}$. All the calculations were done with the correct spin factor.

[13]E. A. Silverstein, Nucl. Instrum. Methods **4,** 53 (1959).

[14]L. H. Johnston and D. A. Swenson, Phys. Rev. **111,** 212 (1958).

[15]D. K. Olsen, Ph.D. thesis, University of Minnesota, 1970 (unpublished); D. K. Olsen and R. E. Brown, Nucl. Phys. **A170,** 544 (1971).

[16]J. Cerny, R. H. Pehl, and G. T. Garvey, Phys. Lett. **12,** 234 (1964).

[17]The following phase conventions are used: (i) Spherical harmonics have Condon-Shortly phases; (ii) $\vec{l} + \vec{s} = \vec{j}$ instead of $\vec{s} + \vec{l} = \vec{j}$; and (iii) radial wave functions start off positive at the origin independent of l.

[18]A. Bohr and B. R. Mottleson, K. Dan. Vidensk. Selsk. Mat.-Fys. Medd. **27** (16), ,(1953).

[19]J. Bardeen, L. N. Cooper, and J. R. Schrieffer, Phys. Rev. **108,** 1175 (1957); N. N. Bogoliubov, Nuovo Cimento **7,** 794 (1958); J. G. Valatin, Nuovo Cimento **7,** 843 (1958).

[20]R. de Swiniarski, A. D. Bacher, F. G. Resmini, G. R. Plattner, D. L. Hendrie, and J. Raynal, Phys. Rev. Lett. **28,** 1139 (1972).

[21]S. G. Nilsson, K. Dan. Vidensk. Selsk. Mat.-Fys. Medd. **29** (16), ,(1955).

[22]K. H. Bhatt, Nucl. Phys. **39.** 375 (1962).

[23]B. F. Bayman and A. Kallio, Phys. Rev. **156,** 1121 (1967).

[24]T. Tamura and T. Udagawa, Technical Report No. 30, Center of Nuclear Studies, University of Texas, 1972 (unpublished).

[25]B. A. Watson, P. P. Singh, and R. E. Segel, Phys. Rev. **182,** 977 (1969).

[26]F. D. Becchetti, Jr., and G. W. Greenlees, in *Proceedings of the Third International Symposium on Polarization Phenomena in Nuclear Reactions*, edited by H. H. Barschall and W. Haeberli (Univ. Wisconsin Press, Madison, Wisconsin, 1971), p. 682.

[27]E. R. Flynn and O. Hansen, Phys. Lett. **31B,** 135 (1970) and E. R. Flynn, private communication; J. B. Ball, R. L. Auble, and P. G. Roos, Phys. Rev. C **4,** 196 (1971); R. A. Broglia, C. Riedel, and T. Udagawa, Nucl. Phys. **A184,** 23 (1972). Using the notation of Broglia, Riedel, and Udagawa we use $N_0 = 21.5$.

[28]B. F. Bayman and D. H. Feng, Nucl. Phys. **A205,** 513 (1973).